2025 American Control Conference (ACC)
July 8-10, 2025. Denver, CO, USA

Output-Constrained Individual Pitch Control using an Adaptive Leaky Integrator for Wind Turbine Blade Load Reductions

Jesse I.S. Hummel[1], Jens Kober[1], and Sebastiaan P. Mulders[1]

Abstract— **Wind turbines are getting larger to increase power capacity. Their longer blades sample a larger area of the spatially and temporally varying turbulent wind field, leading to increased periodic blade load and fatigue damage over time. Individual pitch control (IPC) has proven effective in alleviating these loads by pitching the blades. Conventional IPC fully attenuates the periodic blade loads, which requires excessive pitching, leading to additional stresses on the pitch system. To balance pitch actuation and load alleviation, bounds can be set on the pitch signal (input-constrained IPC), or on the load (output-constrained IPC). While input-constrained IPC has been abundantly researched, little research has focused on output-constrained IPC and on the trade-off when operating between full IPC and no IPC. Therefore, we propose an output-constrained IPC method using an adaptive leaky integrator. The natural frequency of the leaky integrator is adapted on the error between the reference and resultant blade moment. This allows the control scheme to attain every load alleviation level between full and no IPC. Furthermore, in realistic turbulent wind conditions, operating close to full IPC leads to diminishing returns, showing that the proposed controller achieves a superior trade-off between load reduction and actuator effort.**

I. Introduction

The cost of wind energy has drastically reduced in recent decades, making it a common and established electricity source. This has, in part, been enabled through higher capacity ratings, higher hub heights, and longer blades [1]. However, as wind turbines get larger, their structural components become more flexible and thereby increasingly susceptible to fatigue loading.

Especially blade periodic loads contribute to their material fatigue, and arise due to effects like wind shear, tower shadow, turbulence, and rotor misalignment. These loads can be alleviated by pitching the blades in counteraction to those loads. This method is called individual pitch control (IPC) [2] and could lead to better rotor designs and/or increase the lifespan of the wind turbine [3].

The multiblade coordinate (MBC) transformation [4] is used in most IPC implementations. It converts the flapping moment of the three blades, in the rotating frame, to a collective, tilt, and yaw component of the entire rotor, in the non-rotating frame. The dominant 1P (once-per-revolution) blade loads are projected as steady-state contributions on the tilt and yaw axes, which can then be regulated by two single-input single-output (SISO) controllers, typically integral (I) or proportional-integral (PI) controllers. The resulting control signals are then fed to the inverse MBC transformation to convert them to three periodic pitch commands in the rotating frame. Especially in large, flexible turbines, the tilt and yaw axes are coupled, hindering SISO controller design. The coupling is due to system dynamics, in the form of e.g. actuator and blade dynamics. This coupling can be accounted for by multivariable controller design [2], [5] or by decoupling the tilt and yaw axes, enabling SISO controller design. Decoupling can be achieved through an azimuth offset in the inverse MBC transformation. This was already noted by [2] and was formally analyzed by [6], [7].

When aiming for full load alleviation, IPC requires additional periodic pitching of the blades, leading to increased wear on the pitch actuation system, which has hindered industry adoption [8]. To make IPC more practically feasible, a control method that facilitates the trade-off between load reduction and pitch actuation might form an interesting solution.

One such method described in the literature is input-constrained IPC, where the pitch angle, rate, and/or acceleration are limited by saturating the nonrotating control signals [9]. Alternatively, model predictive control (MPC) can integrate such constraints directly in its optimization problem [10]. Furthermore, a data-driven MPC method called constrained subspace predictive repetitive control (cSPRC) was used for input-constrained IPC [11].

On the other hand, output-constrained IPC sets bounds on the allowable loads and uses the minimal pitch signal necessary to keep the loads within these bounds. This is in contrast to input-constrained IPC where the controller aims for full load alleviation and saturates the pitch signal to a certain maximum. Output-constrained IPC ensures that when the loads are already naturally within the bounds in the current wind conditions, the controller converges to no IPC action.

Despite its potential, output-constrained IPC has received little attention in the literature. The authors of [12] use an MBC-based IPC scheme and set a positive bound on only the tilt moment under the assumption that the yaw moment is generally smaller. Furthermore the data-driven cSPRC method has also been demonstrated to achieve output-constrained IPC [13]. In [14], we proposed the ℓ^∞-IPC and ℓ^2-IPC output-constrained IPC controllers using the MBC transformation. However, both control methods need a model-based estimate of the "open-loop load". In this work, we augment our previous work with a model-free control method using classical control theory elements through the following contributions:

[1]Delft University of Technology, Mekelweg 2, 2628 CD Delft, the Netherlands {j.i.s.hummel, j.kober, s.p.mulders}@tudelft.nl

C.1 Proposing and motivating the use of a leaky integrator to enable output-constrained IPC;
C.2 Deriving a general transfer function for output-constrained IPC controllers in the rotating frame for frequency domain analysis, controller design, and calibration;
C.3 Inferring a scheduling function to achieve linear properties from the scheduling parameter to closed-loop performance;
C.4 Analyzing the working mechanism of the proposed scheme in mid-fidelity wind turbine simulations using OpenFAST using laminar wind conditions and showing effectiveness in realistic turbulent wind conditions;
C.5 Analyzing the trade-off when operating anywhere between no IPC and full IPC.

The paper is structured as follows: First, the assumptions underlying this work are discussed. Sect. II then discusses the theory behind the MBC transformation in its relation to IPC. Sect. III presents the adaptive leaky integrator control method of which results are presented in Sect. IV. This paper is concluded in Sect. V.

Assumptions

This work is based on the following assumptions:

A.1 The IPC controllers target the 1P harmonic blade load but could be easily extended to nP, where $n \in \mathbb{N}$.
A.2 The wind turbines are three-bladed ($B = 3$).
A.3 The pitch actuators actuate at the 1P frequency, which is assumed to be well below the actuation bandwidth, justifying neglecting the actuator dynamics.
A.4 The optimal decoupling azimuth offset ψ_o is calculated for a single operating condition, and it is assumed that the wind turbine operates closely enough to this.

II. Individual Pitch Control with the Multiblade Coordinate Transformation

This section discusses the general theory behind the multiblade coordinate transformation, including decoupling of the orthogonal tilt and yaw axes using the azimuth offset.

A. General MBC Theory

The MBC transformation is used in most IPC implementations, and a block diagram of such an implementation is shown in Fig. 1. The forward MBC transformation demodulates the periodic signals originating from the wind turbine linear parameter-varying plant $G(s, \psi)$ (where ψ denotes the azimuth angle) into steady-state contributions, which classical controllers can easily control. The forward MBC transformation for 1P load signals for three blades (in accordance with Assumptions A.1 and A.2) is given as

$$\boldsymbol{M}_{\mathrm{N}}(t) = \frac{2}{3}\begin{bmatrix} 1/2 & 1/2 & 1/2 \\ \cos(\psi_1(t)) & \cos(\psi_2(t)) & \cos(\psi_3(t)) \\ \sin(\psi_1(t)) & \sin(\psi_2(t)) & \sin(\psi_3(t)) \end{bmatrix} \boldsymbol{M}_{\mathrm{R}}(t), \tag{1}$$

where $\boldsymbol{M}_{\mathrm{N}} = \begin{bmatrix} M_0 & M_{\mathrm{t}} & M_{\mathrm{y}} \end{bmatrix}^\top$ are the nonrotating blade moments consisting of the collective, tilt, and yaw flapping moments, ψ_b the azimuth position of blade $b \in [1, B]$ (in accordance with Assumption A.2), and $\boldsymbol{M}_{\mathrm{R}} = \begin{bmatrix} M_1 & M_2 & M_3 \end{bmatrix}^\top$ and contains the flapping moments of the three blades in the rotating frame.

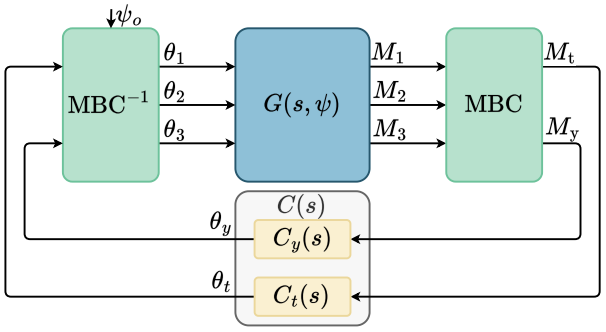

Fig. 1: Block diagram of a conventional IPC implementation using the MBC transformation and two decoupled SISO controllers to fully attenuate the tilt and yaw moments.

Note that due to the presence of nP harmonics in $\boldsymbol{M}_{\mathrm{R}}$, $\boldsymbol{M}_{\mathrm{N}}$ is not a pure steady-state signal but also has power at $3n$P, where $n \in \mathbb{N}$. Furthermore, for unbalanced rotors, the signal would contain power at all nP frequencies [15], [16]. Furthermore, due to turbulence and other stochastic effects on $\boldsymbol{M}_{\mathrm{R}}$, $\boldsymbol{M}_{\mathrm{N}}$ can have power at any frequency. To isolate the steady-state contribution, $\boldsymbol{M}_{\mathrm{N}}$ is usually low-pass filtered.

Typically, two I or PI-controllers are used in a diagonal controller structure, so $C(s) = \mathrm{diag}(C_{\mathrm{t}}(s), C_{\mathrm{y}}(s))$, and aim for complete attenuation of the tilt and yaw moments by generating a tilt and yaw pitch angle.

The resulting tilt and yaw pitch angles are subsequently transformed back to the rotating frame, with the inverse MBC transformation

$$\boldsymbol{\theta}_{\mathrm{R}}(t) = \begin{bmatrix} 1 & \cos(\psi_1(t) + \psi_{\mathrm{o}}) & \cos(\psi_1(t) + \psi_{\mathrm{o}}) \\ 1 & \cos(\psi_2(t) + \psi_{\mathrm{o}}) & \cos(\psi_2(t) + \psi_{\mathrm{o}}) \\ 1 & \cos(\psi_3(t) + \psi_{\mathrm{o}}) & \cos(\psi_3(t) + \psi_{\mathrm{o}}) \end{bmatrix} \boldsymbol{\theta}_{\mathrm{N}}(t), \tag{2}$$

where $\boldsymbol{\theta}_{\mathrm{R}} = \begin{bmatrix} \theta_1 & \theta_2 & \theta_3 \end{bmatrix}^\top$ contains the pitch angles of the three blades in the rotating frame, $\psi_{\mathrm{o}} \in \mathbb{R}$ the azimuth offset, and $\boldsymbol{\theta}_{\mathrm{N}} = \begin{bmatrix} \theta_0 & \theta_t & \theta_y \end{bmatrix}^\top$ contains the collective, tilt, and yaw pitch angles in the nonrotating frame.

B. Frequency Domain Analysis

For controller design and calibration, the plant can be analyzed in the nonrotating domain by using the MBC transformations in the Laplace domain. The derivations are given by [5], [6], from which the main results are given here. The frequency domain representation of the forward transformation is given by

$$\boldsymbol{\mathcal{M}}_{\mathrm{N}}(s) = \frac{2}{3} C_{\mathrm{L}} \boldsymbol{\mathcal{M}}_{\mathrm{R}}(s_-) + \frac{2}{3} C_{\mathrm{H}} \boldsymbol{\mathcal{M}}_{\mathrm{R}}(s_+), \tag{3}$$

and the inverse transformation is given by

$$\boldsymbol{\Theta}_{\mathrm{R}}(s) = \tilde{C}_{\mathrm{L}}^\top(\psi_{\mathrm{o}}) \boldsymbol{\Theta}_{\mathrm{N}}(s_-) + \tilde{C}_{\mathrm{H}}^\top(\psi_{\mathrm{o}}) \boldsymbol{\Theta}_{\mathrm{N}}(s_+), \tag{4}$$

where C_{L} and C_{H} denote the *low* and *high* partial transformation matrices respectively, $\tilde{C}_{\mathrm{L}}^\top(\psi_{\mathrm{o}})$ and $\tilde{C}_{\mathrm{H}}^\top(\psi_{\mathrm{o}})$ the

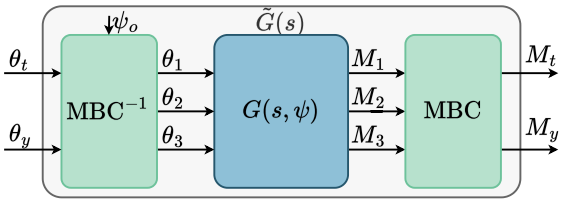

Fig. 2: Block diagram of the demodulated plant $\tilde{G}(s)$. By calibrating the azimuth offset ψ_o, the cross-coupling from θ_t and θ_y to M_y and M_t respectively, is minimized.

transpose of the partial transformation matrices including azimuth offset, and $s_\pm = s \pm j\omega_\mathrm{r}$ and denotes the frequency-shifted Laplace operator.

The block diagram for the demodulated plant is shown in Fig. 2. The demodulated plant $\tilde{G}(s)$ is a linear time-invariant system obtained by averaging out the azimuth dependency of the linear parameter-varying plant $G(s,\psi)$ after transforming it to the nonrotating frame using the MBC transformation. Due to system dynamics, there is coupling between the tilt and yaw inputs and outputs. To enable the use of SISO controllers, the system needs to be decoupled.

C. Decoupling using the Optimal Azimuth Offset

Phase lag in the system, due to e.g. actuator dynamics, blade dynamics, dynamic induction, and communication delays, leads to coupling in the nonrotating frame. Especially for large flexible wind turbines, this coupling is significant and needs to be taken into account during controller design.

Besides multivariable controller design [2], [5], the azimuth offset in the reverse MBC transformation can also be used to decouple the system, enabling the application of two decoupled SISO control loops [6], [7]. The optimal decoupling azimuth offset is found by analyzing the open-loop transfer function of the demodulated plant $\tilde{G}(s)$, shown in Fig. 2, where only the components that are linked to periodic loads (the tilt and yaw inputs and outputs) are shown. This 2×2 system shall have a low gain of the off-diagonal component around the targeted frequencies when effectively decoupled. The next section proposes a novel control method enabling output-constrained IPC.

III. Output-Constrained IPC with an Adaptive Leaky Integrator

This section proposes and motivates the use of an adaptive leaky integrator for output-constrained IPC and shows its working mechanism in the frequency domain, thereby providing Contributions C.1 to C.3.

A. Leaky Integrator

A leaky integrator has high similarities with a pure integrator, but gradually "leaks" a portion of the accumulated signal over time, preventing the output to rise indefinitely, and its transfer function is given by

$$C_\mathcal{L}(s) = \frac{K}{\omega_\mathcal{L} + s}, \tag{5}$$

where K denotes the gain and $\omega_\mathcal{L}$ the natural frequency of the leaky integrator. The Bode magnitude plot for different values of $\omega_\mathcal{L}$ is shown in Fig. 3a, where $\omega_\mathcal{L} = 0$ is equivalent to a pure integrator. By varying $\omega_\mathcal{L}$, the steady-state gain of the leaky integrator can be adjusted, while, crucially, the crossover frequency (if defined) and high-frequency gain stay constant. This is in contrast to varying the natural frequency of a low-pass filter, which causes the filter to change its crossover frequency while its unity steady-state gain remains constant.

Since the DC-gain is finite, the controller causes a finite attenuation of steady-state errors. In the context of IPC: a leaky integrator drives the loads in the nonrotating frame to some nonzero value, reaching any load level between full and no IPC, thus achieving output-constrained IPC.

B. Frequency Domain Analysis in the Rotating Frame

This section extends the frequency response in the nonrotating frame shown in Fig. 3a, with an analysis of the "modulated controller" (controller in the rotating frame) shown in Fig. 4. To derive the transfer function from $\boldsymbol{\mathcal{M}}_\mathrm{R}$ to $\boldsymbol{\Theta}_\mathrm{R}$, we define the equation for the controller output

$$\boldsymbol{\Theta}_\mathrm{N}(s) = \mathrm{diag}(C_t(s), C_y(s))\boldsymbol{\mathcal{M}}_\mathrm{N}(s). \tag{6}$$

Assuming that the tilt and yaw controllers are decoupled and have equal structure and tuning, so $C_t(s) = C_y(s) = c(s)$,

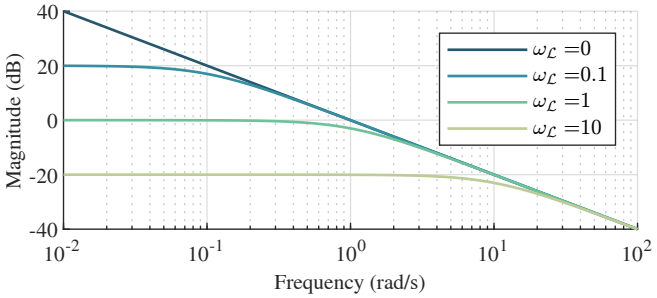

(a) The leaky integrator $C_\mathcal{L}(s)$ in the nonrotating domain.

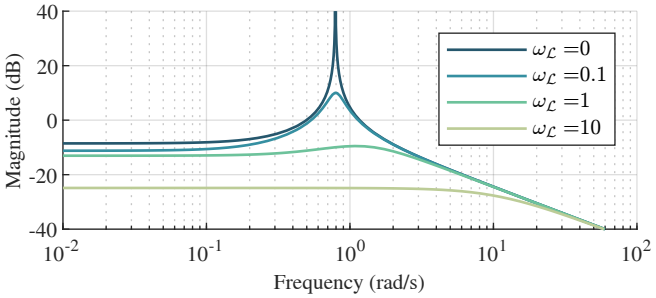

(b) The modulated leaky integrator $\tilde{C}_\mathcal{L}(s)$ in the rotating domain.

Fig. 3: Bode magnitude plot of the leaky integrator for different values of $\omega_\mathcal{L}$ and $K = 1$. By changing $\omega_\mathcal{L}$, the DC-gain of the controller in the nonrotating frame is adjusted (a), and the 1P amplification of the controller in the rotating frame (b).

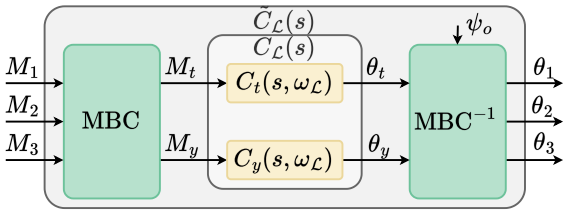

Fig. 4: Block diagram of the modulated controller $\tilde{C}_{\mathcal{L}}(s)$, showing the controller acting from the individual blade loads to the individual pitch actions.

then combining (6) with (3) and (4) leads to

$$\begin{aligned}\boldsymbol{\Theta}_{\mathrm{R}}(s) = \frac{2}{3}\left(c(s_-)\tilde{C}_{\mathrm{L}}^{\top}(\psi_{\mathrm{o}})C_{\mathrm{H}} + c(s_+)\tilde{C}_{\mathrm{H}}^{\top}(\psi_{\mathrm{o}})C_{\mathrm{L}}\right)\boldsymbol{\mathcal{M}}_{\mathrm{R}}(s) \\ + \frac{2}{3}c(s_-)\tilde{C}_{\mathrm{L}}^{\top}(\psi_{\mathrm{o}})C_{\mathrm{L}}\boldsymbol{\mathcal{M}}_{\mathrm{R}}(s_{2-}) \\ + \frac{2}{3}c(s_+)\tilde{C}_{\mathrm{H}}^{\top}(\psi_{\mathrm{o}})C_{\mathrm{H}}\boldsymbol{\mathcal{M}}_{\mathrm{R}}(s_{2+}),\end{aligned}$$

which is simplified using $\tilde{C}_{\mathrm{L}}^{\top}(\psi_{\mathrm{o}})C_{\mathrm{L}} = 0\ \forall\,\psi_{\mathrm{o}} \in \mathbb{R}$ and $\tilde{C}_{\mathrm{H}}^{\top}(\psi_{\mathrm{o}})C_{\mathrm{H}} = 0\ \forall\,\psi_{\mathrm{o}} \in \mathbb{R}$, leading to

$$\begin{aligned}\tilde{C}(s) &= \frac{\boldsymbol{\Theta}_{\mathrm{R}}(s)}{\boldsymbol{\mathcal{M}}_{\mathrm{R}}(s)} \\ &= \frac{2}{3}\left(c(s_-)\tilde{C}_{\mathrm{L}}^{\top}(\psi_{\mathrm{o}})C_{\mathrm{H}} + c(s_+)\tilde{C}_{\mathrm{H}}^{\top}(\psi_{\mathrm{o}})C_{\mathrm{L}}\right),\end{aligned} \tag{7}$$

which denotes the transfer function of a general modulated controller. Substituting the frequency-shifted leaky integrator

$$C_{\mathcal{L}}(s_{\pm}) = \frac{K}{\omega_{\mathcal{L}} + s \pm j\omega_{\mathrm{r}}}, \tag{8}$$

for $c(s_{\pm})$ in (7), a 3×3 system for the modulated leaky integrator in the rotating domain is derived. The Bode magnitude plot from the first blade moment to the first blade pitch for different values of $\omega_{\mathcal{L}}$ is shown in Fig. 3b. The modulated controller is thus a second-order system with a variable damping ratio based on $\omega_{\mathcal{L}}$. When $\omega_{\mathcal{L}} = 0$, the controllers behave as pure integrators in the nonrotating frame, resulting in an infinite gain at the 1P frequency of the modulated controller in the rotating frame, leading to complete attenuation of the 1P loads in the closed-loop system. For increasing $\omega_{\mathcal{L}}$, the targeted 1P gain decreases so that finite attenuation of the 1P load is achieved.

C. Implementation in Output-Constrained IPC

As concluded in the previous section, by adjusting $\omega_{\mathcal{L}}$, any level between no and full IPC can be achieved. To adjust $\omega_{\mathcal{L}}$, an adaptation function f compares a load reference with the resultant magnitude of the tilt/yaw moment and changes $\omega_{\mathcal{L}}$ accordingly. The resulting block diagram for the proposed output-constrained IPC controller using an adaptive leaky integrator is shown in Fig. 5. Like conventional IPC, each axis is regulated by its own controller, which are both adapted with the same $\omega_{\mathcal{L}}$.

D. Leaky Integrator Adaptation

The adaptation function f adjusts $\omega_{\mathcal{L}}$ to operate between no and full IPC in order to follow a reference load. However, the relation between the level of IPC and $\omega_{\mathcal{L}}$ is nonlinear. So the relation between the closed-loop performance and $\omega_{\mathcal{L}}$ is analyzed to ensure consistent operation. The closed-loop, steady-state performance is given by

$$T(0) = \frac{L(0)}{1 + L(0)} = \frac{K\tilde{G}(0)}{\omega_{\mathcal{L}} + K\tilde{G}(0)}, \tag{9}$$

where T denotes the closed-loop transfer function and L the loop gain. This equation can be rewritten to

$$\omega_{\mathcal{L}} = K\tilde{G}(0)\left(\frac{1}{T(0)} - 1\right), \tag{10}$$

which thus specifies to required natural frequency of the leaky integrator $\omega_{\mathcal{L}}$ as a function of the desired closed-loop, steady-state performance. The closed-loop, steady-state performance $T(0)$ is equal to the obtained IPC level on a scale from 0 (no IPC) to 1 (full IPC). So, (10) gives the relation between the desired IPC level and $\omega_{\mathcal{L}}$. To obtain the desired IPC level, the load error is integrated, resulting in the following adaptation function

$$\omega_{\mathcal{L}} = f(e) = K\tilde{G}(0)\left(\frac{1}{K_{\mathrm{i}}\int e\mathrm{d}t} - 1\right), \tag{11}$$

where e is the load error defined as

$$e = r - \left\| \begin{bmatrix} M_{\mathrm{t}} \\ M_{\mathrm{y}} \end{bmatrix} \right\|_2, \tag{12}$$

where r denotes the reference load. Note that (11) is a differential equation but deviates from the standard adaptation

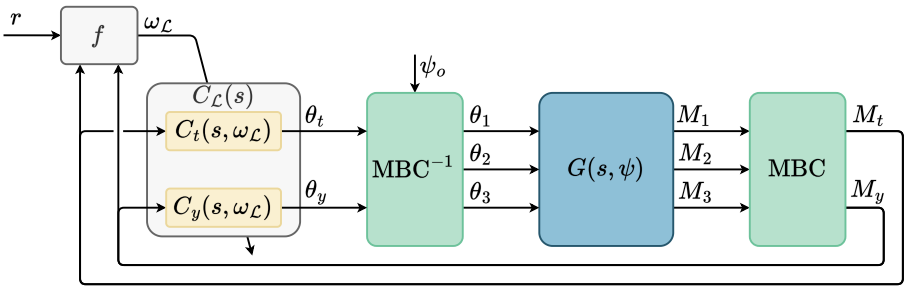

Fig. 5: Block diagram of the proposed output-constrained IPC controller. The MBC transformation projects the individual blade loads to the nonrotating frame which are then regulated by two leaky integrators. An adaptation function f adapts $\omega_{\mathcal{L}}$ to follow a given load reference r for the resultant magnitude of the tilt-yaw moment.

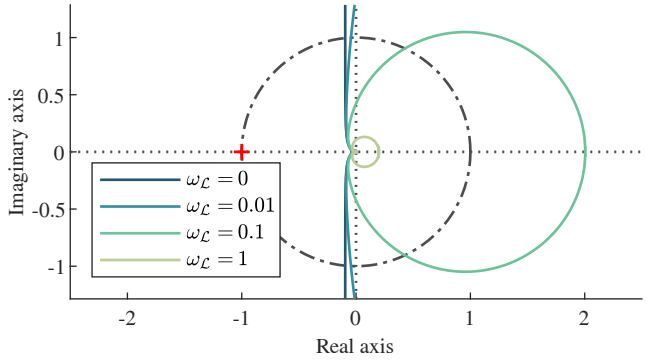

Fig. 6: Nyquist plot of the loop transfer function showing that the closed-loop system is stable for $\omega_\mathcal{L} \geq 0$.

law form by calculating $\omega_\mathcal{L}$ directly instead of its derivative. Effectively, (11) adjusts $\omega_\mathcal{L}$ more slowly in regions where the sensitivity on closed-loop performance with respect to changes in control parameters is high and slower where this sensitivity is small. This ensures smooth transitions between different operating levels. In addition, to avoid dividing by zero in (11), the integrator saturation lower bound is set equal to 0.001 (0.1 %), which makes the controller practically equal to no IPC. Furthermore, the upper bound is 1 (100 %), corresponding to full IPC. The closed-loop system is stable within this saturated range $0.001 \leq \omega_\mathcal{L} \leq 1$, because it is stable for any positive value of $\omega_\mathcal{L}$, as demonstrated in the next section.

IV. Results

This section discusses the calibration of the controller and presents results from the mid-fidelity wind turbine simulator OpenFAST [17] simulations on the IEA 15 MW turbine [18]. Two sets of simulations were run at above-rated conditions, at a wind speed of 15 m/s. The first set of simulations is in laminar wind conditions, providing Contribution C.4, and the second set in realistic turbulent conditions, providing Contributions C.4 and C.5.

A. Controller Calibration

Three parameters need to be calibrated: the azimuth offset ψ_o, leaky integrator gain K, and adaptation gain K_i.

Using the procedure outlined in Sect. II-C, the optimal decoupling azimuth offset for the IEA 15 MW reference turbine at an operating point of 15 m/s is found to equal 26.4° for the 1P harmonic without actuator dynamics (in accordance with Assumptions A.1 and A.3). The azimuth offset can be scheduled to account for the change in wind speed due to turbulence [19], but a single operating point is assumed in this work (Assumption A.4).

The gain K determines the crossover frequency of the leaky integrator and can thus be tuned using the conventional IPC tuning method. By transforming the plant to the nonrotating domain, shown in Fig. 2, a crossover frequency of the loop gain of 0.2 rad/s is targeted, resulting in a gain of $K = 1.17 \times 10^{-6}$. The Nyquist plot for the loop transfer function is shown in Fig. 6, and shows a gain margin of 32.4 dB and phase margin of 84.6° when $\omega_\mathcal{L} = 0$. Furthermore, as $\omega_\mathcal{L}$ increases, the stability margins increase, showing that the system is stable for $\omega_\mathcal{L} \geq 0$.

An adaptation gain value of $K_i = -5 \times 10^{-5}$ was found to result in satisfactory controller performance.

B. Laminar Conditions

In laminar conditions, the working mechanisms of the controller can be demonstrated. To analyze the response of the controller, the reference load is lowered every 40 seconds towards zero. Fig. 7a shows the flapping moment after it has been band-pass filtered around the 1P frequency and the pitch angle in the rotating frame. The magnitude of the load follows the reference accurately by increasing the magnitude of the pitch angle. But crucially, the controller does not amplify the load towards the reference when the load is naturally below it. Thus, it never increases the fatigue loads on the blades. Fig. 7b shows the same signals but in the nonrotating frame. The magnitude of the nonrotating load accurately follows the reference by increasing the nonrotating

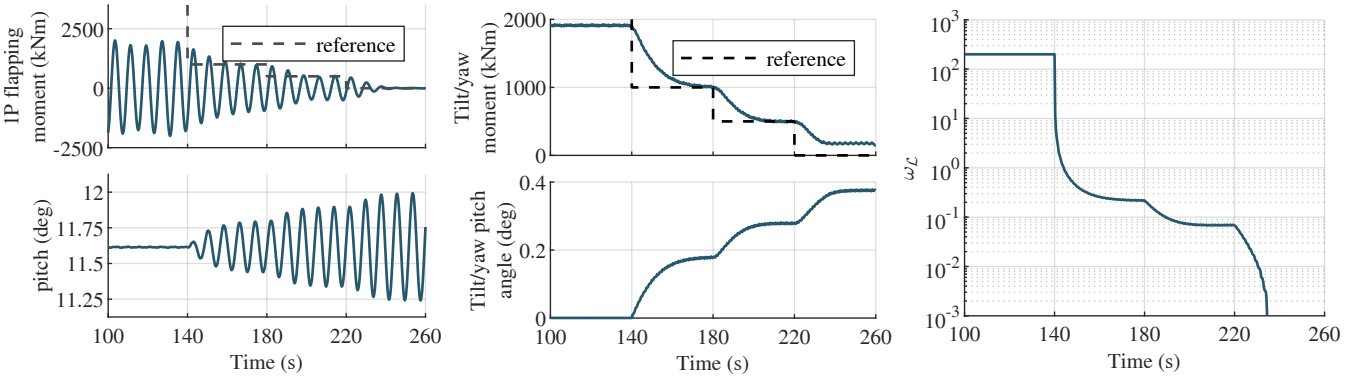

(a) Rotating frame. (b) Nonrotating frame. (c) Natural frequency of the leaky integrator.

Fig. 7: Simulation in laminar condition with a staircase load reference. The load and pitch amplitude are shown in the rotating frame (a) and nonrotating frame (b). As $\omega_\mathcal{L}$ decreases (c), the adaptive leaky integrator reduces the 1P component of the flapping load further to keep it on the reference load (a, b).

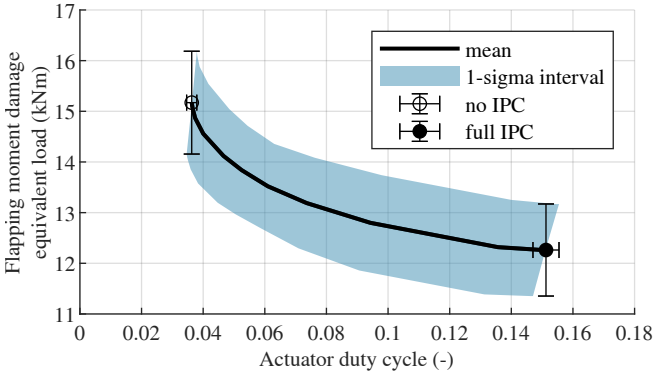

Fig. 8: Trade-off between DEL and ADC in turbulent flow conditions. The initial reduction in DEL is high, but operating closer to full IPC leads to diminishing returns.

pitch angle. Initially, the controller operates at an IPC level of 0.1 % due to the integrator saturation bounds by having a high value for $\omega_{\mathcal{L}}$, shown in Fig. 7c. The adjustment of $\omega_{\mathcal{L}}$ is quite nonlinear but occurs smoothly and without overshoot due to the adaptation function (11), which finally sets $\omega_{\mathcal{L}}$ to zero when enabling full IPC.

C. Turbulent Conditions

This section analyzes the trade-off between no and full IPC in realistic wind conditions with a turbulence intensity of 8 %. To get a statistically meaningful result, 30-minute simulations with 17 different reference loads and 8 different random seeds for the synthetic turbulence were run. The damage equivalent load (DEL) of the flapping moment and the actuator duty cycle (ADC) were calculated for each run. The average and the standard deviation over all random seeds are shown in Fig. 8. The reduction in DEL is initially large for a small increase in ADC. However, when operating close to full IPC, the additional ADC leads to diminishing returns. So, output-constraint IPC with a moderate reference on the load yields a better trade-off between DEL and ADC.

V. Conclusions

In this work, an adaptive leaky integrator is proposed to achieve output-constrained IPC with the MBC transformation. The natural frequency of the leaky integrator determines the amount of attenuation of the periodic blade loads and is adjusted using an adaptation function that tracks a tilt/yaw moment reference but never amplifies the loads. The controller can operate on any operating point between no and full IPC, thus facilitating the trade-off between load reduction and pitch actuation. Furthermore, operating close to full IPC leads to diminishing returns in the trade-off between DEL and ADC, showing that the proposed scheme achieves a superior trade-off between load reduction and actuator effort. As this output-constrained IPC scheme is an extension of well-established IPC schemes, it enables the industry to use the benefits of IPC without excessive actuator wear. Future work will focus on how to optimally calibrate this control method to find the Pareto front between DEL and ADC.

Code Availability

The code repository used for this work can be found at `https://doi.org/10.5281/zenodo.15024224`.

References

[1] P. Veers, K. Dykes, E. Lantz, S. Barth, C. Bottasso, O. Carlson, A. Clifton, J. Green, P. Green, H. Holttinen, D. Laird, V. Lehtomäki, J. Lundquist, J. Manwell, M. Marquis, C. Meneveau, P. Moriarty, X. Munduate, M. Muskulus, J. Naughton, L. Pao, J. Paquette, J. Peinke, A. Robertson, J. Rodrigo, A. Sempreviva, J. Smith, A. Tuohy, and R. Wiser, "Grand challenges in the science of wind energy," *Science*, 2019.

[2] E. A. Bossanyi, "Individual Blade Pitch Control for Load Reduction," *Wind Energy*, 2003.

[3] T. Burton, N. Jenkins, D. Sharpe, E. Bossanyi, and M. Graham, *Wind Energy Handbook*, 3rd ed. Hoboken, NJ: Wiley, 2021.

[4] G. Bir, "Multi-Blade Coordinate Transformation and its Application to Wind Turbine Analysis," in *46th AIAA Aerospace Sciences Meeting and Exhibit*, 2008.

[5] Q. Lu, R. Bowyer, and B.Ll. Jones, "Analysis and design of Coleman transform-based individual pitch controllers for wind-turbine load reduction: Individual blade-pitch control," *Wind Energy*, 2015.

[6] S. P. Mulders, A. K. Pamososuryo, G. E. Disario, and J. W. van Wingerden, "Analysis and optimal individual pitch control decoupling by inclusion of an azimuth offset in the multiblade coordinate transformation," *Wind Energy*, 2019.

[7] S. P. Mulders and J. W. van Wingerden, "On the Importance of the Azimuth Offset in a Combined 1P and 2P SISO IPC Implementation for Wind Turbine Fatigue Load Reductions," in *American Control Conference (ACC)*, 2019.

[8] E. J. Novaes Menezes, A. M. Araújo, and N. S. Bouchonneau Da Silva, "A review on wind turbine control and its associated methods," *Journal of Cleaner Production*, 2018.

[9] R. Ungurán, V. Petrović, L. Y. Pao, and M. Kühn, "Smart rotor control of wind turbines under actuator limitations," in *American Control Conference (ACC)*, 2019.

[10] V. Petrović, M. Jelavić, and M. Baotić, "MPC framework for constrained wind turbine individual pitch control," *Wind Energy*, 2021.

[11] Y. Liu, R. Ferrari, and J. W. van Wingerden, "Periodic Load Rejection for Floating Offshore Wind Turbines via Constrained Subspace Predictive Repetitive Control," in *American Control Conference (ACC)*, 2021.

[12] A. Henry, M. Pusch, and L. Pao, "Investigation of $\mathscr{H}_\infty$-Tuned Individual Pitch Control for Wind Turbines," *Wind Energy*, 2024.

[13] Y. Liu, R. Ferrari, and J. W. van Wingerden, "Load reduction for wind turbines: An output-constrained, subspace predictive repetitive control approach," *Wind Energy Science*, 2022.

[14] J. I. S. Hummel, J. Kober, and S. P. Mulders, "Output-constrained individual pitch control methods using the multiblade coordinate transformation: Trading off actuation effort and blade fatigue load reduction for wind turbines," *Wind Energy Science (in review)*, 2025.

[15] S. Kanev and T. van Engelen, "Exploring the Limits in Individual Pitch Control," in *European Wind Energy Conference and Exhibition, EWEC*, 2009.

[16] E. van Solingen and J. W. van Wingerden, "Linear individual pitch control design for two-bladed wind turbines," *Wind Energy*, 2015.

[17] B. Jonkman, R. M. Mudafort, A. Platt, E. Branlard, M. Sprague, H. Ross, J. Jonkman, HaymanConsulting, M. Hall, D. Slaughter, G. Vijayakumar, M. Buhl, Russell9798, P. Bortolotti, Reos-Rcrozier, Shreyas Ananthan, S. Michael, J. Rood, Rdamiani, Nrmendoza, Sinolonghai, Pschuenemann, Ashesh2512, Kshaler, S. Housner, Psakievich, K. Bendl, L. Carmo, E. Quon, and Mattrphillips, "OpenFAST v3.5.0," Zenodo, 2023.

[18] E. Gaertner, J. Rinker, L. Sethuraman, F. Zahle, B. Anderson, G. Barter, N. Abbas, F. Meng, P. Bortolotti, W. Skrzypinski, G. Scott, R. Feil, H. Bredmose, K. Dykes, M. Shields, C. Allen, and A. Viselli, "IEA Wind TCP Task 37: Definition of the IEA 15-Megawatt Offshore Reference Wind Turbine," National Renewable Energy Laboratory (NREL), 2020.

[19] M. Lara, S. P. Mulders, J. W. van Wingerden, F. Vázquez, and J. Garrido, "Analysis of Adaptive Individual Pitch Control Schemes for Blade Fatigue Load Reduction on a 15 MW Wind Turbine," *Applied Sciences*, 2024.